The TATA-Binding Protein Core Domain in Solution Variably Bends TATA Sequences via a Three-Step Binding Mechanism†

Roberto F. Delgadillo, JoDell E. Whittington, Laura K. Parkhurst, and Lawrence J. Parkhurst*

Department of Chemistry, University of Nebraska, Lincoln, Nebraska 68588-0304

Received October 3, 2008; Revised Manuscript Received December 15, 2008

ABSTRACT: Studies of the binding and bending of the AdMLP TATA sequence (TATAAAAG) by the core domain of yeast TBP allow quantitation of the roles of the N-terminal domains of yeast and human TBP. All three proteins bind DNA via a three-step mechanism with no evidence for an initially bound but unbent DNA. The large enthalpy and entropy of activation for the first step in ***y***TBP binding can now be assigned to movement of the NTD from the DNA binding pocket and not to energetics of DNA bending. The energetic patterns for ***h***TBP and ***c***TBP suggest that the 158-amino acid NTD in ***h***TBP does not initially occupy the DNA binding pocket. Despite the appearance of similar energetics for ***h***TBP and ***c***TBP, order of magnitude differences in rate constants lead to differing populations of intermediates during DNA binding. We find that the NTDs destabilize the three bound forms of DNA for both ***y***TBP and ***h***TBP. For all three proteins, the DNA bend angle (θ) depends on the TATA sequence, with θ for ***c***TBP and ***h***TBP being greater than that for ***y***TBP. For all three proteins, θ for the G6 variant (TATAAGAG) varies with temperature and increases in the presence of osmolyte to be similar to that of AdMLP. Crystallographic studies of ***c***TBP binding to a number of variants had shown no dependence of DNA bending on sequence. The results reported here reveal a clear structural difference for the bound DNA in solution versus the crystal; we attribute the difference to the presence of osmolytes in the crystals.

Binding of the TATA-binding protein (TBP)[1] to the promoter TATA box (TATAa/tAa/t) is central to transcription initiation by polymerases I, II, and III (*1*−*3*). Promoter recognition occurs through sequential reactions with formation of two stable TBP−DNA_{TATA} intermediate complexes for both ***y***TBP_{wt} (*4*−*6*) and ***h***TBP_{wt} (*7*). The resulting TBP_{wt}−promoter complexes accommodate a broad range of helical bending from 29.9° to 97.0° depending on the TATA sequence (*8, 9*) and protein species (*7*). In crystalline complexes, the DNA-binding COOH-terminal domain (***c***TBP) by itself induces an ∼80° helical bend in DNA_{TATA} independent of the TBP species (*8, 10*−*13*) or TATA sequence (*14*).

Comparisons of results obtained using the conserved ***c***TBP and the native protein, which includes a highly heterogeneous NH_2-terminal domain, show differences in self-assembly (*15*−*18*) and in DNA binding and bending (*19*−*24*). Evidence from fluorescence and protein footprinting studies of ***y***TBP suggests modulation of the ***c***TBP by NH_2-terminal domain occupation of the DNA binding site in competition with promoter binding (*23, 25*). Because these collective studies have variously utilized either the yeast or human proteins under diverse conditions and approaches, determining which of the constituent elements of promoter binding and bending are inherent to the COOH-terminal domain in a solution environment has not been possible.

We have thus conducted a rigorous biophysical study of ***c***TBP interacting with promoter DNA_{TATA} and compared the results to those of related studies utilizing the full-length human (*7, 26*) and yeast TBPs (*4, 5, 8, 9, 27*). Fluorescence resonance energy transfer (FRET)-based experiments included steady-state and time-resolved emission together with FRET stopped-flow and stopped-flow anisotropy. The two-intermediate reaction mechanism for promoter binding is shown to be an intrinsic property of the core domain based on a global analysis of the combined equilibrium and association and relaxation kinetics data. The accompanying energetic changes are remarkably similar to those of ***h***TBP but not ***y***TBP. Even so, differences in the microscopic rate constants lead to significantly different reaction progressions for ***c***TBP and ***h***TBP. The severe bend angle of 95° induced by ***c***TBP in the consensus adenovirus major late promoter (AdMLP) is likewise similar to the ***h***TBP-induced bend. Notably, ***c***TBP-induced bends in five variant TATA sequences range from 43° to 95°, demonstrating that, in a solution environment, the core domain accommodates a range of bend angles just like the native proteins ***c***TBP and ***h***TBP.

† The work was supported by NIH Grants GM59346 and RR015468.

* To whom correspondence should be addressed. Telephone: (402) 472-3316. Fax: (402) 472-2044. E-mail: lparkhurst1@unl.edu.

[1] Abbreviations: TBP, TATA-binding protein with ***c***, ***y***, and ***h*** denoting core, yeast, and human, respectively; AdMLP, adenovirus major late promoter; PIC, preinitiation complex; CTD, COOH-terminal domain; NTD, NH_2-terminal domain; FRET, fluorescence resonance energy transfer; T, TAMRA or *N*,*N*,*N*′,*N*′-tetramethyl-6-carboxyrhodamine; Xr, x-rhodamine; F, fluorescein; Xr(T)*$AdMLP_{dpx}$*F, 14 bp DNA duplex (5′-CGCTATAAAAGGGC-3′) bearing the 8 bp AdMLP TATA sequence, with 5′-Xr or T and 3′-F on the top strand; °$AdMLP_{dpx}$°, unlabeled 14 bp DNA duplex.

10.1021/bi8018724 CCC: $40.75
Published on Web 02/06/2009

In addition, at 15 °C, for the G6 promoter bound to ***c***TBP, the bend angle increases from 75° to 91° as the glycerol concentration is increased to 3 M. For AdMLP, there is virtually no effect of glycerol on the bend angle. These results point to the presence of osmolytes as the primary source of the differences in bending reported for complexes in crystals (*14*).

EXPERIMENTAL PROCEDURES

TBP−DNA_{TATA} recognition mechanisms and the concurrent induced helical bending have been a primary research focus in our laboratory for more than a decade (*4, 5, 7*−*9, 26*−*28*). These solution studies utilize DNA oligomers having fluorescent dyes attached to either end of the coding strand and employ an array of biophysical methods. Because the experiments and analyses herein were intentionally conducted to conform to those performed previously with ***y***TBP and ***h***TBP and various TATA sequences, brief summaries are provided with references and any differences are noted explicitly.

Materials and Solution Conditions. The primary probe was identical to the probe used in our ***y***TBP (*4*) and ***h***TBP (*7, 26*) studies. This 14 bp DNA oligomer bearing the adenovirus major later promoter (5′-CGC**TATAAAAG**GGC-3′) has 3′-carboxy-fluorescein (F) as the donor dye for the singly and doubly labeled probe and 5′-TAMRA (T) or X-rhodamine (Xr) as the acceptor dye for the doubly labeled oligo, with both dyes attached to the top strand via linker arms (http://www.trilinkbiotech.com). Four analogous oligomers doubly labeled with 3′-F and 5′-Xr and bearing AdMLP variant sequences were utilized in time-resolved experiments: G6, TATAAGAG; T6, TATAATAG; C7, TATAAACG; and A3, TAAAAAAG. The labeled and unlabeled coding strands and their complementary strands were synthesized by Trilink Biotechnologies, Inc. (San Diego, CA), and purified by HPLC and PAGE, with purity confirmed in our laboratory by comparing the molar absorptivity ratios in the UV and visible regions. The T*/Xr*$AdMLP_{dpx}$*F notation refers to a duplex, which was formed by adding at least 10-fold excess complement to ensure >99% hybridization (*29*) of the labeled strand (binding of the duplex to TBP was unaltered when the concentration of the single-strand complement was increased to 100 times the concentration of the labeled top strand).

Experiments were conducted at the indicated temperatures in 25 mM Tris, 100 mM KCl, 5 mM $MgCl_2$, 1 mM $CaCl_2$, and 2 mM DTT at pH 8, the latter to ensure the presence of a single fluorescein species (*30*). ***c***TBP was used at very low concentrations, up to 165 nM, to favor the monomeric species under the conditions used herein (*23*), and the reported TBP concentrations are for the active protein.

Protein Activity and Association Constants. The COOH-terminal domain of ***y***TBP from *Saccharomyces cerevisiae* was expressed in *Escherichia coli*, purified, and concentrated in 25 mM HEPES-KOH, 20% glycerol, 1 mM EDTA, 1 mM DTT, and 300 mM KCl (pH 7.9) (*23*) and was the generous gift of M. Brenowitz. The protein activity (α) and the ***c***TBP−DNA_{AdMLP} binding constant were carefully determined using several independent methods to ensure accuracy and meaningful comparisons with ***y***TBP and ***h***TBP. Xr*$AdMLP_{dpx}$*F (25 nM) was first titrated with 0−400 nM ***c***TBP at 15 °C with nine points per curve, monitoring the change in the steady-state emission of the donor fluorescein as described previously (*4,5,7,26,31*). A 20 °C binding curve was also obtained using the intrinsic tyrosine fluorescence of the protein, which is quenched upon DNA binding (*23*). Core TBP (500 nM) was titrated with unlabeled DNA_{AdMLP} at 12 concentrations ranging from 0 to 700 nM using 278 nm excitation and with emission monitored at 306 nm. These collective titration data were used to obtain the association equilibrium constants together with the protein activity (*7*).

A temperature transition experiment was then conducted, and the data were analyzed as described previously (*7*). Briefly, 19 nM ***c***TBP and 20 nM Xr*$AdMLP_{dpx}$*F were equilibrated at 10 °C, and the steady-state emission spectrum was collected. The temperature was then increased by 5 °C increments, and spectra were obtained following equilibration up to 25 °C. The observed emission changes yielded K_a values at each temperature. A van't Hoff plot was constructed using these values together with those obtained from the titrations; least-squares analysis yielded the value of $\Delta H°$ and the optimal K_a values at each of the four temperatures.

Association and Relaxation Kinetics. Association kinetic reactions were monitored using a temperature-controlled stopped-flow apparatus as described with excitation from a Coherent (Santa Clara, CA) Ar^+ ion laser (Innova 70-4 Argon) tuned to 488 nm and using 15−20 mW of power (*4, 5, 7, 27*). FRET stopped-flow association curves were obtained for the ***c***TBP-Xr*$AdMLP_{dpx}$*F interaction at 15, 20, and 25 °C using 20 nM duplex DNA and protein concentrations of 43, 86, and 165 nM at each temperature (concentrations are after mixing), with donor emission collected at 520 nm through an interference filter (Oriel Corp., Stratford, CT). The sample was subjected to excitation light continuously for the initial ∼35 s of the reaction and then at 4−10 s intervals every 80−160 s until the reaction was more than 95% complete at 15 °C or 100% complete at 20 and 25 °C. Three or five decays were collected at each temperature and ***c***TBP concentration with 1530 data points per second. Each trace was baseline corrected and fitted to bi- and triexponential models. The resultant amplitude changes and eigenvalues describing the kinetics for each condition were averaged to yield nine stopped-flow association curves. The association kinetics were also obtained using anisotropy stopped-flow as described for $\boldsymbol{h}TBP_{wt}$ (*7*), following the time course of changes in the rotational mobility of Xr as 20 nM Xr*$AdMLP_{dpx}$ bound to 49 nM ***c***TBP at 20 °C.

The relaxation constant, *R*, describing the rate of relaxation of the system from one equilibrium state to another, was obtained by challenging equilibrated ***c***TBP-Xr*$AdMLP_{dpx}$*F solutions with a large excess of unlabeled $AdMLP_{dpx}$ (°$AdMLP_{dpx}$°) at 15, 20, and 25 °C. The labeled complex was formed with 22 nM Xr*$AdMLP_{dpx}$*F and 58 nM ***c***TBP, ensuring more than 91% duplex saturation at all temperatures that were sampled. The subsequent replacement of labeled by unlabeled $AdMLP_{dpx}$ in the binary complex was monitored using steady-state FRET as described previously (*7*). Donor emission was collected

intermittently during the first 90 s of the reaction to reduce the level of exposure of the sample to the excitation light. Spectra were then collected every 4−10 min until the reaction was complete, for a total of 10−15 scans. Relaxation curves were obtained at all three temperatures for °$AdMLP_{dpx}$° concentrations of 1, 5, and 9.6 μM.

Binding Mechanism Determination Using Global Analysis of Combined Data. A simple one-step model could be eliminated a priori on the basis of the complexity of the observed association and relaxation kinetics. The ability of a two-step, one-intermediate model to accommodate the data ensemble was evaluated using a set of three linear relationships based on the observed eigenvalues, as detailed elsewhere (*7*).

The ***c***TBP−DNA_{AdMLP} equilibrium and kinetic data were then globally analyzed using both one- and two-intermediate models as follows:

$$\boldsymbol{c}\text{TBP} + \text{DNA} \underset{k_2}{\overset{k_1}{\rightleftarrows}} (\boldsymbol{c}\text{TBP}\cdots\text{DNA})_{\mathbf{I_1}} \underset{k_4}{\overset{k_3}{\rightleftarrows}} \boldsymbol{c}\text{TBP}-\text{DNA}_{\text{final}} \quad (1)$$

$$\boldsymbol{c}\text{TBP} + \text{DNA} \underset{k_2}{\overset{k_1}{\rightleftarrows}} (\boldsymbol{c}\text{TBP}\cdots\text{DNA})_{\mathbf{I_1}} \underset{k_4}{\overset{k_3}{\rightleftarrows}} (\boldsymbol{c}\text{TBP}\cdots\text{DNA})_{\mathbf{I_2}} \underset{k_6}{\overset{k_5}{\rightleftarrows}} \boldsymbol{c}\text{TBP}-\text{DNA}_{\text{final}} \quad (2)$$

with $\mathbf{I_1}$ and $\mathbf{I_2}$ denoting unique ***c***TBP−DNA conformers. These analyses included the sets of nine stopped-flow association kinetic curves and three relaxation decays together with the three equilibrium constants and have been described in detail (*4, 5, 27*). As in our ***h***TBP analysis (*7*), the integration routines were for non-pseudo-first-order conditions. The one-intermediate model (eq 1) was analyzed for the four microstate rate constants (k_i), the four corresponding activation energies, and the quantum yield of the donor fluorescein in each of the two bound species relative to that in the unbound labeled duplex DNA. The parameters for the two-intermediate model included the six rate constants and activation energies and the relative quantum yield values for $\mathbf{I_1}$, $\mathbf{I_2}$, and the TBP−DNA_{final} complex. As an additional constraint on the fitting, both analyses incorporated the variable amplitudes from the stopped-flow association data, which derived from the use of nonsaturating ***c***TBP concentrations. Overall binding constant information thus derived from both amplitudes and from rate constants. Thirty initial starting positions in multidimensional parameter space were employed in a Simplex algorithm to obtain the optimal parameter values. Parameter errors were determined as described previously (*7*). Transition-state theory was used to calculate the associated stepwise enthalpy and entropy changes. Finally, two statistical tests were conducted to compare the appropriateness of the one- and two-intermediate models to this data ensemble.

Interdye Distance Distributions and Corresponding Bend Angles. 3′-Donor−5′-acceptor distances were determined from fluorescence decays resolved in the nanosecond time regime using a LaserStrobe spectrofluorometer (PTI, Photon Technologies, Inc., Birmingham, NJ) with 10 Hz pulsed excitation as described previously (*5, 8, 9, 29*). Briefly, 20 nM $AdMLP_{dpx}$*F, $Xr*AdMLP_{dpx}$*F, $T*AdMLP_{dpx}$*F, or one of four doubly labeled variant duplexes were saturated with ***c***TBP at 20 °C. $T*AdMLP_{dpx}$*F was included to afford a direct comparison with the ***y***TBP- and ***h***TBP-induced bend angles determined previously (*7, 8*). Donor excitation was at 481 nm using PLD481 dye (Photon Technologies, Inc.) with donor emission collected at 520 nm through a 520 nm interference filter (Oriel Corp.) preceded by a 1 cm path length liquid filter containing 24.1 mM acetate-buffered dichromate (pH 4) to remove scattered light. Three successive replicate decays were collected and immediately averaged to yield one sample decay having 120 points with 30 excitation pulses per point. Six sample curves and two instrument response function curves, obtained using a glycogen solution, composed a set; at least four sets per sample were collected.

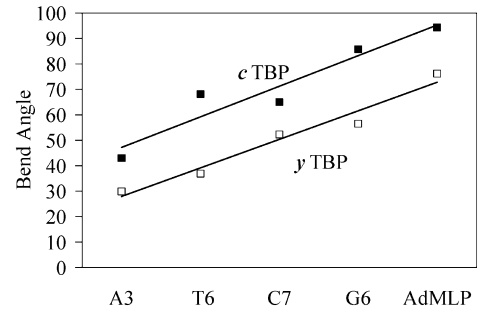

FIGURE 1: Broad range of bend angles induced in consensus and variant TATA sequences by the TBP core domain at 20 °C in solution. The filled squares represent data for ***c***TBP whereas the empty squares designate data for ***y***TBP (*8*), previously reported to have bend angles ranging from 29.9° to 76.2°.

The decay curves were fitted to mono-, bi-, and triexponential decay models using the PTI iterative reconvolution software program based on the Marquardt algorithm (*32*). Model selection depended on the values of χ^2, the Durbin-Watson parameter, which reflects residual correlation (*33*), and the runs test (*34*). The optimal theoretical curves were used to obtain the mean 3′-donor−5′-acceptor distance, $\bar{R}$, and the corresponding width of the distance distribution (σ) for each TATA sequence using the method of moments (*35*). DNA bend angles were determined from these distance distributions using a simple bending model as described previously (*7*−*9, 36*). The simple two-kink rod model for DNA only requires interdye distances for free and bound DNA. We are in the process of determining the actual phasing of the dyes which will allow more detailed considerations of DNA kinking, unwinding, and changes in the dihedral angle of the distorted DNA in TBP.

RESULTS

Highly Variable ***c****TBP-Induced* DNA_{TATA} *Bend Angles in Solution.* The mean 3′-donor−5′-acceptor distances, $\bar{R}$, for ***c***TBP-bound AdMLP and the four variant TATA sequences differed over a significant range: AdMLP, 51.0 Å; G6, 53.3 Å; T6, 55.9 Å; C7, 58.1 Å; and A3, 62.0 Å. These mean end-to-end distances yield bend angles at 20 °C that vary over a range of 50°: AdMLP, 95°; G6, 85.8°; T6, 68.1°; C7, 65°; and A3, 43° (Figure 1). Notably, these results establish DNA sequence-dependent promoter bending as an inherent characteristic of the core domain.

c*TBP*−DNA_{AdMLP} *Binding, Association and Relaxation Kinetics.* van't Hoff analysis of the combined titration and temperature transition data gave K_d values at 10, 15, 20, and

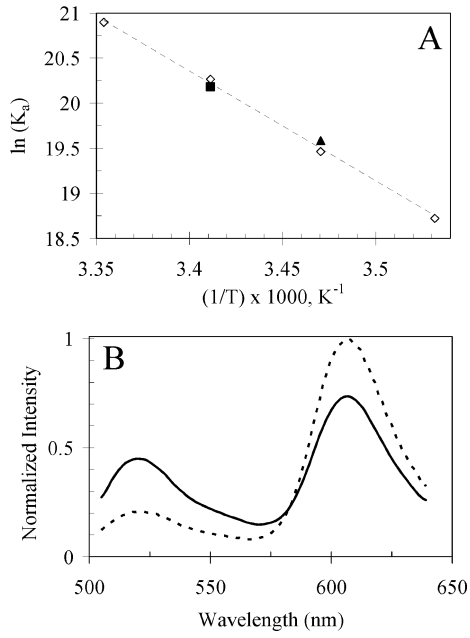

FIGURE 2: (A) van't Hoff plot of the combined ***c***TBP−DNA_{AdMLP} titration and temperature transition data. The K_a values obtained from the FRET (▲) and tyrosine (■) titrations together with those obtained from the temperature transitions (◇) were subjected to regression analysis to obtain the optimal values reported in the text at 10, 15, 20, and 25 °C. (B) Corresponding corrected emission spectra of unbound (—) and bound (---) xR*$AdMLP_{dpx}$*F are shown. The spectra of unbound and fully bound xR*$AdMLP_{dpx}$*F and of unbound and fully bound $AdMLP_{dpx}$*F are invariant over the experimental temperature range (*4, 7*).

25 °C of 7.14 ± 0.25, 3.40 ± 0.05, 1.65 ± 0.02, and 0.82 ± 0.03 nM, respectively, with a $\Delta H°$ value of 24.2 ± 1.2 kcal/mol (Figure 2). The steady-state amplitude of the donor emission decreased 53% with full ***c***TBP saturation. The ***c***TBP activity was determined as described to be 28%. For G6, the amplitude changes from ~43% to 53% after addition of 3 M glycerol at 15 °C.

The kinetic traces monitoring the association of the Xr*$AdMLP_{dpx}$*F population with ***c***TBP were biphasic with the fast phase rate and amplitude increasing from 0.05 s^{-1} for the lowest temperature and concentration (15 °C and 42 nM ***c***TBP, respectively), comprising 43% of the total amplitude change, to 0.16 s^{-1}, reflecting 68% of the amplitude change for the highest temperature and concentration (25 °C and 162 nM ***c***TBP, respectively). The observed total amplitude changes over the experimental range of temperatures and protein concentrations varied from 50.4% to 53% with the latter reflecting maximum saturation, in exact agreement with the corresponding change observed in the steady state. Amplitude changes of <53% derived from reactions that were not driven to completion under the experimental conditions. Overall half-times for the reactions ranged from 25 s at 15 °C and 42 nM ***c***TBP to 3 s at 25 °C and 165 nM ***c***TBP. In Figure 3, we show a comparison of the association reactions for ***c***TBP, ***y***TBP, and ***h***TBP. The corresponding trace at 20 °C obtained using stopped-flow anisotropy was also biphasic with a fast phase identical within error to that of the stopped-flow FRET curve (Figure 4). This observation reflects the absence of detectable initial association of ***c***TBP with unbent DNA, as elaborated in Discussion. The measured replacement rate of labeled by

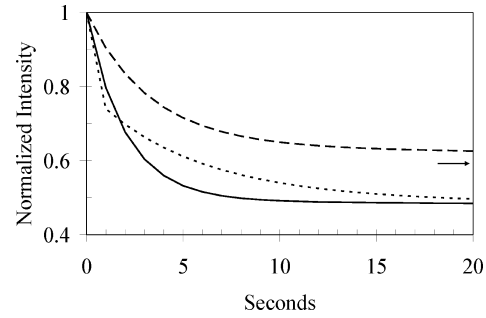

FIGURE 3: Theoretical stopped-flow FRET association curves calculated using the best fitting parameters derived from global fitting according to the three-step mechanism (*4, 7*). The curves are for 20 °C, with 20 nM DNA and 400 nM protein: ***c***TBP (—), ***h***TBP (•••), and ***y***TBP (---). A biphasic profile is observed in each case with fluorescence changes of 42% for ***y***TBP and ~52% for ***h***TBP and ***c***TBP, which are proportional to the calculated bend angles of 77° and 95−97°, respectively. The arrow denotes the end point for the final very slow phase for **y**TBP.

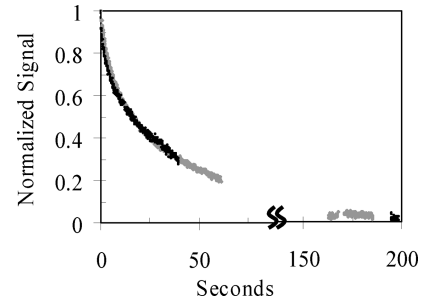

FIGURE 4: Comparison of the normalized observed raw stopped-flow FRET (gray points) and raw stopped-flow anisotropy (black points) association curves at 20 °C for 49 nM ***c***TBP. This experiment emphasized the first phase of the reaction. The excitation light beam was blocked during the time gaps in data collection to minimize photobleaching. The rates of the fast phases are identical within error: 0.34 ± 0.015 and 0.35 ± 0.02 s^{-1}, respectively. That these two experimental curves proceed at the same initial rate precludes a mechanism in which ***c***TBP binds to unbent DNA, as discussed in the text. Note that for both FRET and anisotropy, the normalized signal, $\hat{S}$, is $(S_t - S_\infty)/(S_0 - S_\infty)$; however, the FRET signal decreases with time, whereas the anisotropy increases with time.

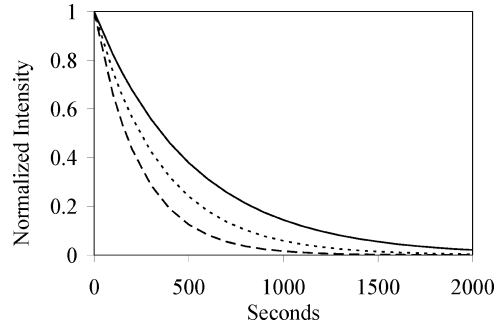

FIGURE 5: Measured relaxation rate for the replacement of labeled by unlabeled DNA_{AdMLP} in the equilibrated ***c***TBP-xR*$AdMLP_{dpx}$*F complex, which was inversely dependent on temperature: 25 (—), 20 (•••), and 15 °C (---) with corresponding monophasic decays of 0.0019 ± 0.0001, 0.0029 ± 0.0002, and 0.0042 ± 0.0002 s^{-1}, respectively.

unlabeled $AdMLP_{dpx}$ in the ***c***TBP-Xr*$AdMLP_{dpx}$*F complex was temperature-dependent (Figure 5). The additional dependence on the concentration of unlabeled DNA revealed the presence of second-order displacement in addition to pure first-order replacement. Facilitated dis-

placement also occurs in ***y***TBP complexes with the E4 promoter sequence and with the C7 TATA sequence (*5, 27*). However, ***y***TBP−DNA and ***h***TBP−DNA complexes bearing AdMLP relax only through replacement (*4, 7*), distinguishing the core from the two-domain proteins. Extrapolation at each temperature of the measured rate constant to zero °$AdMLP_{dpx}$° gave pure replacement constants of 0.0042, 0.0028, and 0.0019 s^{-1} at 15, 20, and 25 °C, respectively (Figure 5). The implications of such an inverted temperature dependence have been discussed (*7*). In the case of ***c***TBP, $R \approx k_2k_4k_6/k_3k_5$, and the inverted temperature dependence derives solely from the large activation energy for k_5, transformation of $\mathbf{I_2}$ to the final complex. The 53% amplitude change observed for these relaxation curves is in agreement with those for the association kinetics and the equilibrium binding curves.

Quantitative Recognition Pathway for ***c****TBP−DNA$_{AdMLP}$ Binding and Bending.* A one-intermediate model was eliminated on the basis of the striking lack of a common intersection point inside positive rate constant space for the three linear relationships described in Experimental Procedures (data not shown). Both the information theoretic test (AIC) of Akaike (*37, 38*) and the modified *F* test (*39, 40*) use the ratio of χ_ν^2 values, which was 0.45 for the two- versus the one-intermediate model. The AIC test decisively excluded the one-intermediate model. The *F* test overwhelmingly favored the two-intermediate model; even at the 99% confidence level, the one-intermediate model could be considered acceptable only if 97% of the total data points were discarded.

The combined association and relaxation data were very well accommodated by a three-step linear model (eq 2), with all theoretical curves well within the error of the observed curves. The dissociation equilibrium values derived from the global fitting were 3.29 ± 0.05 nM at 15 °C, 1.67 ± 0.02 nM at 20 °C, and 0.82 ± 0.01 nM at 25 °C. These values and those determined experimentally as described in Experimental Procedures and reported above are indistinguishable at the 68% confidence level. The $\Delta H°$ value determined for the association reaction from these globally determined constants is 23.7 ± 1.0 kcal/mol, in excellent agreement with the value of 24.2 ± 1.2 kcal/mol obtained experimentally. The optimal rate constants at 25 °C are listed in Table 1 together with the corresponding thermodynamic values and relative quantum yields.

The sequential thermodynamic changes associated with these partial reactions are shown in Figure 6. A repetitive energetic pattern is apparent in the successive formation of the three binary complexes, $\mathbf{I_1}$, $\mathbf{I_2}$, and ***c***TBP−DNA_{final}: at each step, a decrease in enthalpy is overcome by a corresponding increase in entropy. Initial ***c***TBP−DNA_{AdMLP} binding proceeds over an activation barrier of only 9 kcal/mol to form $\mathbf{I_1}$, which has an enthalpy 4.5 kcal/mol higher and an entropy 50.6 cal K^{-1} mol^{-1} higher than those of the reactants. The second step is similar, requiring 16.5 kcal/mol of activation energy to yield the second intermediate with an enthalpic increase of 7.3 kcal/mol and a commensurate entropic increase of 60.7 cal K^{-1} mol^{-1}. The largest changes occur in the final step, with a steep activation barrier, 20.3 kcal/mol, leading to $\Delta H°$ and $\Delta S°$ increases of 28.7 kcal/mol and 137.4 cal K^{-1} mol^{-1}, respectively. Comparisons with native human and yeast TBP are discussed below.

Table 1: Optimal Rate Constants at 25 °C and Corresponding Enthalpy and Entropy Profiles for ***c***TBP−DNA_{AdMLP} Reaction Steps[a]

	k_i[b]	$\Delta H_i^{\circ\ddagger}$ (kcal/mol)	$\Delta S_i^{\circ\ddagger}$ (cal K^{-1} mol^{-1})[c]
$i = 1$	1.64 [1.58,1.70]	9.1 [8.5,9.7]	−1.56
$i = 2$	0.028 [0.020,0.040]	4.6 [2.0,7.7]	−52.2
$i = 3$	5.4 [4.25,6.55]	5.8 [2.8,9.1]	−37.4
$i = 4$	3.6 [3.02,4.26]	3.1 [1.1,5.1]	−47.5
$i = 5$	0.083 [0.063,0.104]	24.5 [21.1,28.0]	16.7
$i = 6$	0.007 [0.006,0.008]	3.1 [1.7,4.5]	−60
QYI_1	0.55 [0.48,0.62]		
QYI_2	0.51 [0.46,0.56]		
QY_{final}	0.506 [0.50,0.51]		

[a] The values shown are for 25 °C and 1 M standard state and assume $\Delta C_p^{\ddagger} = 0$ for a temperature independence for $\Delta H_i^{\circ\ddagger}$ or $\Delta S_i^{\circ\ddagger}$ in each reaction step *i*. The reported parameter error estimates are averages of those obtained from the variance matrix and simulated noise data fitting. The 15 × 15 variance matrix was calculated as described in ref *7* with the exception that 12 kinetics curves were used (nine stopped-flow association curves and three dissociation curves). Twenty simulated noisy data sets were created by adding random noise of the same magnitude as in the experimental data to obtain the distribution of fitted parameters (*49*). [b] k_1 is a bimolecular rate constant with dimensions of μM^{-1} s^{-1}; the dimensions for k_2-k_6 are s^{-1}. [c] $\Delta S_i^{\circ\ddagger}$ values were calculated with the transition-state theory with k_i and $\Delta H_i^{\circ\ddagger}$.

Species Populations under Optimal Cell Conditions. Simulations conducted at 37 °C using presumed cell concentrations of 10 μM ***c***TBP and DNA (*41, 42*) and the corresponding optimal rate constants show the time evolution of each species along the reaction pathway, for comparison with those for ***y***TBP and ***h***TBP (Figure 7). The most notable feature is the high $\mathbf{I_2}$ concentration, which surpasses the $\mathbf{I_1}$ concentration within 1 s and is unique among the TBP−DNA_{AdMLP} reactions we have characterized (*4, 7*).

DISCUSSION

This work establishes quantitatively the aspects of promoter binding and bending that are inherent to the COOH-terminal domain of TBP with two primary findings. (i) In a solution environment, the core domain by itself induces variable DNA bends from 43° to 95° depending on the TATA sequence, and (ii) a sequential three-step promoter recognition mechanism is a characteristic of the core domain and thus does not result from dynamic interactions among the core domain, the NH_2-terminal domain, and promoter DNA. We have previously discussed the initial binding and bending of DNA by TBP (*7, 28*) and have proposed that distributions of conformers of both the DNA (*28*) and the TBP (*7*) must be considered. From this perspective, energetics associated with k_1 derive in part from linked equilibria among conformers of both DNA and TBP with the subsets of conformers that are appropriately adapted for entering into a productive complex. The observed kinetics in all cases rule out an initially bound but unbent or weakly bent TBP−DNA complex.

Discussion of these results centers on comparisons with native human and yeast TBPs, which have been previously characterized using essentially identical biophysical methods, analyses, and conditions (*4, 5, 7, 26, 31*). Considering ***c***TBP behavior over and against that of ***h***TBP and ***y***TBP provides context and is key for distinguishing the roles of the two domains, characterizing the interdomain dynamics, and

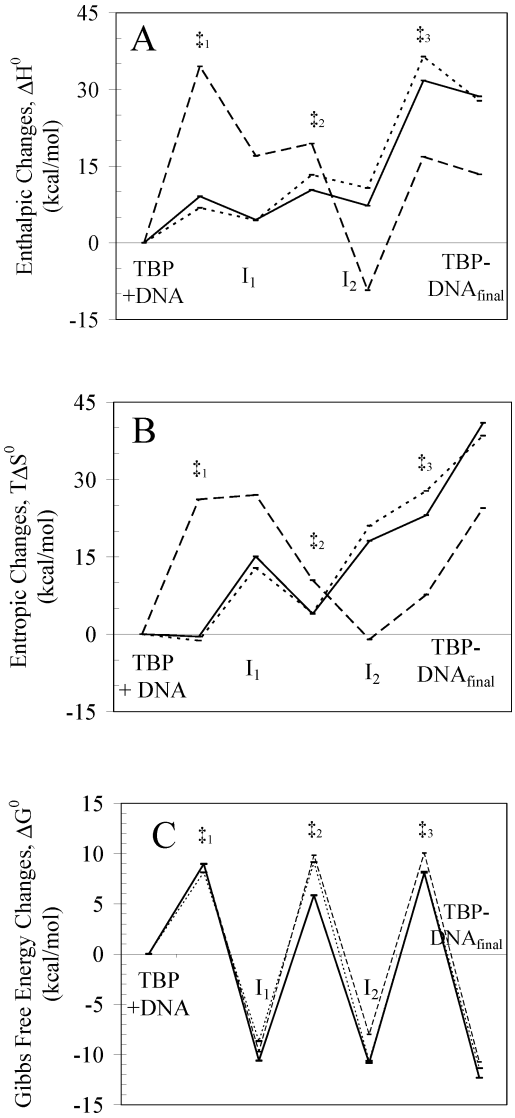

FIGURE 6: Thermodynamic profiles for ***c***TBP, ***h***TBP, and ***y***TBP at 25 °C. The enthalpic progression of the reaction for the core (—), human (•••), and yeast (---) proteins (A) and the corresponding entropic changes $T\Delta S^{\circ\ddagger}$ (B) and free energy change $\Delta G^{\circ\ddagger}$ (C) are shown. The $\ddagger_i$ symbol denotes a transition state for step *i*. The ***y***TBP reaction follows a markedly different energetic course than those of ***c***TBP and ***h***TBP, which have similar patterns.

clarifying the regulatory role of the secondary domain. This comparison assumes that core domains derived from yeast and human are essentially identical, on the basis of crystallographic studies and an 81% homology with nearly 100% conservation of the DNA-contacting residues (*10, 11, 43*).

Most surprising was the strong dependence on the TATA sequence of the ***c***TBP-induced bend angle (Figure 1). This finding contrasts with those obtained from high-resolution studies of crystalline ***c***TBP−DNA$_{TATA}$ complexes that yield ~80° bends independent of TATA sequence (*14*). These results demonstrate that variable bending is an inherent characteristic of the core domain in a solution environment.

The dependence on glycerol concentration of the bend angle in solution for G6 bound to ***c***TBP is strong evidence that crystallographic results showing no sequence dependence (*14*) derived from the effects of osmolytes. Our previous results (*8*) based on full-length ***y***TBP had left unresolved whether the effects of osmolytes were directly affecting the core domain or were mediated through the NTD.

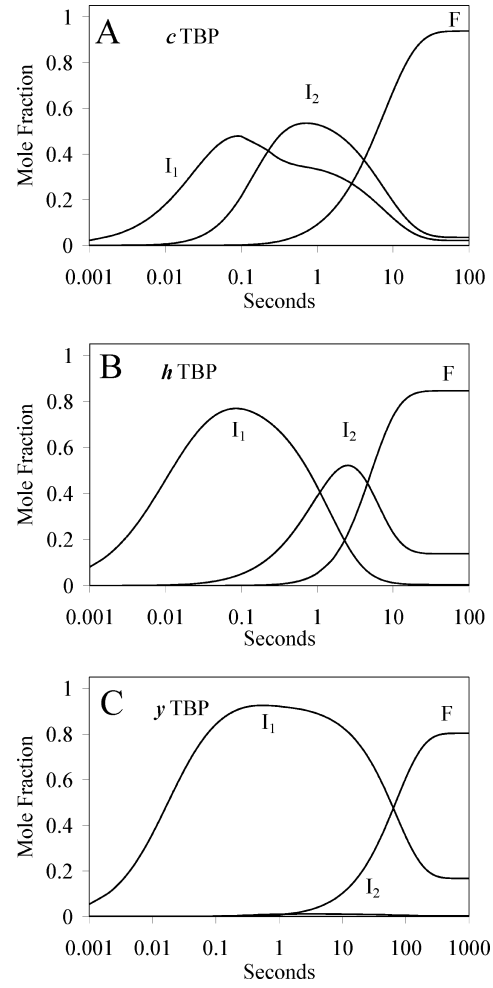

FIGURE 7: Time evolution of the reactive species for the ***c***TBP−DNA$_{AdMLP}$ reaction at 37 °C (A) for 10 μM protein and DNA. The dominance of $\mathbf{I_2}$ over $\mathbf{I_1}$ for ***c***TBP distinguishes this reaction from those of ***h***TBP [B (*7*)] and ***y***TBP [C (*4*)], in which $\mathbf{I_1}$ prevails and remains present in the yeast reaction in significant mole fractions at equilibrium. At 37 °C, ***y***TBP reaches equilibrium ~10 times more slowly than either ***h***TBP or ***c***TBP.

Also surprising were the nearly identical ***c***TBP- and ***h***TBP$_{wt}$-induced bending of AdMLP, 95° and 97°, respectively. The general picture that has emerged is for a "super" core domain that is differentially modulated by the highly heterologous NH_2-terminal domains, which range in length from four amino acids for *Pyrococcus woesi* (*44*) to 158 amino acid for *Homo sapiens* (*45*). The expectation was therefore that the core domain by itself would induce the most severe bend. In fact, the presence of the large ***h***TBP NH_2-terminal domain has almost no effect on the strong bend imposed by the primary domain. The ***h***NTD may have evolved to be so large to preclude occupancy of the binding site to optimize transcription efficiency, leaving as its primary role mediation of subsequent protein−protein interactions.

In contrast, ***y***TBP induces an 82° bend in DNA$_{AdMLP}$ (*7, 8*), a substantial modulation of the severe distortion observed with ***c***TBP and ***h***TBP of 95° and 97°, respectively. The variable bending induced in the nonconsensus promoter sequences likewise differs between full-length ***y***TBP and ***c***TBP (Figure 1). The ***y***NTD must be responsible for the differences. With these short oligomers, we see no evidence of an interaction between the NH_2-terminal domain and the duplex-linked dyes that would indicate direct ***y***NTD-DNA

Table 2: Comparative Rate Constants for ***c***TBP, ***h***TBP, and ***y***TBP Corresponding to eq 2 for 25 °C

	k_i (s^{-1})[a]		
	cTBP	***h***TBP[b]	***y***TBP
$i = 1$	1.64 [1.58,1.70]	6.8 [6.4,6.9]	1.59 [1.56,1.66]
$i = 2$	0.028 [0.020,0.04]	3.0 [2.8,3.4]	0.118 [0.114,0.125]
$i = 3$	5.4 [4.25,6.55]	0.54 [0.51,0.57]	0.0288 [0.0283,0.0339]
$i = 4$	3.64 [3.02,4.26]	0.020 [0.015,0.025]	0.541 [0.534,1.01]
$i = 5$	0.083 [0.063,0.104]	0.096 [0.053,0.141]	0.365 [0.365,0.730]
$i = 6$	0.007 [0.006,0.008]	0.029 [0.024,0.034]	0.00354 [0.00349,0.00395]

[a] Rate constants shown are at 25 °C. k_1 is a bimolecular rate constant with dimensions of μM^{-1} s^{-1}. [b] ***h***TBP data at 20 °C were used to calculate values at 25 °C from values for $\Delta H^{\circ\ddagger}$ (*7*).

contact. However, repositioning of the ***y***NTD atop the convex surface of the ***y***CTD upon DNA binding (*23*−*25*) may inhibit the core domain's "hinge motion" and thus the extent of bending in ***y***TBP.

Functionally, it is of particular note that a three-step recognition mechanism (eq 2) describes the ***c***TBP−DNA_{AdMLP} reaction. This general binding mechanism, with two intermediate TBP−DNA species, is common to both ***h***TBP (*7*) and ***y***TBP (*4*) interacting with DNA_{AdMLP} and to ***y***TBP interacting with the *adenovirus* E4 consensus promoter and a variant sequence (*5, 27*). These results show that this complex reaction is inherent to the COOH-terminal domain and does not arise from a dynamic interaction among the core, the NH_2-terminal domain, and the DNA during promoter binding and bending.

The pattern of energetic changes along the reaction pathway differs significantly between the ***y***TBP and ***c***TBP reactions (Figure 6). These differences imply modulation of the three-step mechanism by the ***y***NTD. Unexpected was the similarity between these energetic changes between ***c***TBP and ***h***TBP (Figure 6). Even so, an examination of the free energy changes for formation of $\mathbf{I_1}$, $\mathbf{I_2}$, and the final complex from the reactants shows that, in every instance, the presence of either the yeast or human NTD destabilizes the binary complexes from 15 to 25 °C.

To understand how these reactions unfold, it is necessary to consider the kinetics as well as the energetics: the microscopic rate constants determine the populations and rates of formation of the intermediate and final species along the reaction coordinate. Three of the six microscopic rate constants (k_2, k_3, and k_4) differ by orders of magnitude between ***c***TBP and ***h***TBP (Table 2 and Figure 7), leading in turn to substantially different evolution of the intermediates during the binding process (Figure 7). These differences derive from the small differences in $\Delta H^{\circ\ddagger}$ and $T\Delta S^{\circ\ddagger}$, which are magnified because they are noncompensating and because these energy terms appear in an exponential in the rate constant expression. Again, these differences must be attributable to the ***h***NTD.

The two-intermediate pathway has been confirmed for the ***y***TBP reaction by single-molecule experiments (*6*) and for ***h***TBP (*7*), ***y***TBP (*4*), and ***c***TBP (Figure 4) by stopped-flow anisotropy. Anisotropy is a linear function of concentration when there is no change in the fluorescence of the emitting dye. A rapid phase corresponding to an initial detectable binding without bending would be revealed by a faster phase in the stopped-flow anisotropy compared to the stopped-flow FRET. No such additional rapid phase has been detected. The biphasicity of both the stopped-flow FRET and stopped-flow anisotropy curves derives from an initial pre-steady-state phase reflecting the equilibrium between free DNA and DNA bound in $\mathbf{I_1}$ that pauses the system, followed by a slower steady-state progression of the system through the intermediates.

Additionally, ***c***TBP, $\boldsymbol{h}TBP_{wt}$, and $\boldsymbol{y}TBP_{wt}$ all induce a strong bend in the first TBP−DNA_{AdMLP} intermediate complex along the three-step reaction pathway, as reflected in the relative quantum yield of $\mathbf{I_1}$ in each case, 0.55, 0.52, and 0.547, respectively (*4, 7*). There is thus no evidence for an initial shallow bend followed by an isomerization to strongly bent DNA. We have proposed previously that the high activation barrier leading to $\mathbf{I_1}$ in the ***y***TBP reaction might be related to energetic requirements for bending DNA to fit into the binding saddle (*4, 28*). These comparative studies reveal that this is not the case, since very low energy barriers for both core and ***h***TBP result in $\mathbf{I_1}$ with strongly bent DNA. The collective data point instead to ***y***NTD displacement from the binding pocket as the source of the high activation energy in the initial step of the yeast reaction (*4, 24, 46*). This view predicts a very low value for k_1. Because k_1 is in fact very similar for all three proteins (Table 2 and Figure 6), the high initial ***y***TBP−DNA_{AdMLP} energy barrier must be offset by a large positive activation entropy (*4*) associated with the inter-domain dynamics. The similar fitted quantum yields for the three intermediates within each of the three TBP proteins suggest only small structural differences at the DNA binding site. We have recently reported, however, using rapid-mixing with nanosecond time-resolved FRET that the bend angle in ***y***TBP $\mathbf{I_1}$ is ∼10° greater than in the final complex, and that the fluorescence of W26 in the N-terminal domain shows three distinct states in ***y***TBP (*47*). We suggest that transitions among the three bound DNA forms of ***c***TBP will drive the displacements of the N-terminal domains of ***y***TBP and ***h***TBP.

We have proposed previously that $\boldsymbol{y}\mathbf{I_1}$ (*4, 5*) and $\boldsymbol{h}\mathbf{I_1}+\boldsymbol{h}\mathbf{I_2}$ (*7*) are the biologically relevant complexes, even though the final complex is the most energetically stable in all three cases. The $\mathbf{I_1} \leftrightarrow \mathbf{I_2}$ exchange in the two full-length proteins is much slower than in the core, revealing free energy barriers for these conformational changes that must be due to their respective NTDs. The $\mathbf{I_2}$ to $\mathbf{I_1}$ transition has essentially the same energy barrier for ***c***TBP and ***h***TBP but a very unfavorable entropy for the latter, leading to the much lowered rate constant k_4. The $\mathbf{I_1}$ to $\mathbf{I_2}$ transition (k_3) is 1 order of magnitude faster for ***c***TBP than for ***h***TBP. That difference derives primarily from the associated energy barrier in the ***h***TBP reaction.

From these results, it is clear that NTDs function to mediate affinity, binding rates, the extent of induced bending, and the populations of the intermediate complexes. Each of these effects directly impacts the transcription process. The subsequent binding of additional transcription factors may be influenced by the extent of the bend since a strong correlation is observed between bend angle and transcription efficiency (*8, 48*). The intermediate species have been proposed to be the species upon which the PIC is nucleated, with PIC formation under kinetic rather than thermodynamic control (*4, 7*). Gover-

nance of these species' populations by NTDs is then an additional means of regulating transcription.

ACKNOWLEDGMENT

We thank Professor Michael Brenowitz and Huiyong Cheng for providing core TATA-binding protein.

REFERENCES

1. Hernandez, N. (1993) TBP, a universal eukaryotic transcription factor? *Genes Dev. 7*, 1291–1308.
2. Burley, S. K., and Roeder, R. G. (1996) Biochemistry and structural biology of transcription factor IID (TFIID). *Annu. Rev. Biochem. 65*, 769–799.
3. McKnight, S. L. (1996) Transcription revisited: A commentary on the 1995 Cold Spring Harbor Laboratory meeting, "Mechanisms of Eukaryotic Transcription". *Genes Dev. 10*, 367–381.
4. Parkhurst, K. M., Richards, R. M., Brenowitz, M., and Parkhurst, L. J. (1999) Intermediate species possessing bent DNA are present along the pathway to formation of a final TBP-TATA complex. *J. Mol. Biol. 289*, 1327–1341.
5. Powell, R. M., Parkhurst, K. M., Brenowitz, M., and Parkhurst, L. J. (2001) Marked stepwise differences within a common kinetic mechanism characterize TATA-binding protein interactions with two consensus promoters. *J. Biol. Chem. 276*, 29782–29791.
6. Tolić-Nørrelykke, S. F., Rasmussen, M. B., Pavone, F. S., Berg-Sørensen, K., and Oddershede, L. B. (2006) Stepwise bending of DNA by a single TATA-box binding protein. *Biophys. J. 90*, 3694–3703.
7. Whittington, J. E., Delgadillo, R. F., Attebury, T. J., Parkhurst, L. K., Daugherty, M. A., and Parkhurst, L. J. (2008) TATA-binding Protein Recognition and Bending of a Consensus Promoter are Protein Species Dependent. *Biochemistry 47*, 7264–7273.
8. Wu, J., Parkhurst, K. M., Powell, R. M., Brenowitz, M., and Parkhurst, L. J. (2001) DNA bends in TATA-binding protein-TATA complexes in solution are DNA sequence-dependent. *J. Biol. Chem. 276*, 14614–14622.
9. Wu, J., Parkhurst, K. M., Powell, R. M., and Parkhurst, L. J. (2001) DNA sequence-dependent differences in TATA-binding protein-induced DNA bending in solution are highly sensitive to osmolytes. *J. Biol. Chem. 276*, 14623–14627.
10. Juo, Z. S., Chiu, T. K., Lieberman, P. M., Baikalov, I., Berk, A. J., and Dickerson, R. E. (1996) How proteins recognize the TATA box. *J. Mol. Biol. 261*, 239–254.
11. Kim, Y., Geiger, J. H., Hahn, S., and Sigler, P. B. (1993) Crystal structure of a yeast TBP/TATA-box complex. *Nature 365*, 512–520.
12. Kim, J. L., Nikolov, D. B., and Burley, S. K. (1993) Co-crystal structure of TBP recognizing the minor groove of a TATA element. *Nature 365*, 520–527.
13. Bleichenbacher, M., Tan, S., and Richmond, T. J. (2003) Novel interactions between the components of human and yeast TFIIA/TBP/DNA complexes. *J. Mol. Biol. 332*, 783–793.
14. Patikoglou, G. A., Kim, J. L., Sun, L., Yang, S.-H., Kodadek, T., and Burley, S. K. (1999) TATA element recognition by the TATA box-binding protein has been conserved throughout evolution. *Genes Dev. 13*, 3217–3230.
15. Coleman, R. A., and Pugh, B. F. (1997) Slow dimer dissociation of the TATA binding protein dictates the kinetics of DNA binding. *Proc. Natl. Acad. Sci. U.S.A. 94*, 7221–7226.
16. Daugherty, M. A., Brenowitz, M., and Fried, M. G. (1999) The TATA-binding protein from *Saccharomyces cerevisiae* oligomerizes in solution at micromolar concentrations to form tetramers and octamers. *J. Mol. Biol. 285*, 1389–1399.
17. Campbell, K. M., Ranallo, R. T., Stargell, L. A., and Lumb, K. J. (2000) Reevaluation of Transcriptional Regulation by TATA-Binding Protein Oligomerization: Predominance of Monomers. *Biochemistry 39*, 2633–2638.
18. Daugherty, M. A., Brenowitz, M., and Fried, M. G. (2000) Participation of the Amino-Terminal Domain in the Self-Association of the Full-Length yeast TATA Binding Protein. *Biochemistry 39*, 4869–4880.
19. Horikoshi, M., Yamamoto, T., Ohkuma, Y., Weil, P. A., and Roeder, R. G. (1990) Analysis of structure-function relationships of yeast TATA box binding factor TFIID. *Cell 61*, 1171–1178.
20. Lieberman, P. M., Schmidt, M. C., Kao, C. C., and Berk, A. J. (1991) Two distinct domains in the yeast transcription factor IID and evidence for a TATA box-induced conformational change. *Mol. Cell. Biol. 11*, 63–74.
21. Kuddus, R., and Schmidt, M. C. (1993) Effect of the non-conserved N-terminus on the DNA binding activity of the yeast TATA binding protein. *Nucleic Acids Res. 21*, 1789–1796.
22. Lee, M., and Struhl, K. (2001) Multiple functions of the nonconserved N-terminal domain of yeast TATA-binding protein. *Genetics 158*, 87–93.
23. Gupta, S., Cheng, H., Mollah, A. K., Jamison, E., Morris, S., Chance, M. R., Khrapunov, S., and Brenowitz, M. (2007) DNA and Protein Footprinting Analysis of the Modulation of DNA Binding by the N-Terminal Domain of the *Saccharomyces cerevisiae* TATA Binding Protein. *Biochemistry 46*, 9886–9898.
24. Khrapunov, S., and Brenowitz, M. (2007) Influence of the N-Terminal Domain and Divalent Cations on Self-Association and DNA Binding by the *Saccharomyces cerevisiae* TATA Binding Protein. *Biochemistry 46*, 4876–4887.
25. Rashidzadeh, H., Khrapunov, S., Chance, M. R., and Brenowitz, M. (2003) Solution structure and interdomain interactions of the *Saccharomyces cerevisiae* "TATA binding protein" (TBP) probed by radiolytic protein footprinting. *Biochemistry 42*, 3655–3665.
26. Masters, K. M., Parkhurst, K. M., Daugherty, M. A., and Parkhurst, L. J. (2003) Native human TATA-binding protein simultaneously binds and bends promoter DNA without a slow isomerization step or TFIIB requirement. *J. Biol. Chem. 278*, 31685–31690.
27. Powell, R. M., Parkhurst, K. M., and Parkhurst, L. J. (2002) Comparison of TATA-binding protein recognition of a variant and consensus DNA promoters. *J. Biol. Chem. 277*, 7776–7784.
28. Parkhurst, K. M., Brenowitz, M., and Parkhurst, L. J. (1996) Simultaneous binding and bending of promoter DNA by the TATA binding protein: Real time kinetic measurements. *Biochemistry 35*, 7459–7465.
29. Williams, S. L., Parkhurst, L. K., and Parkhurst, L. J. (2006) Changes in DNA bending and flexing due to tethered cations detected by fluorescence resonance energy transfer. *Nucleic Acids Res. 34*, 1028–1035.
30. Sjöback, R., Nygren, J., and Kubista, M. (1995) Absorption and fluorescence properties of fluorescein. *Spectrochim. Acta, Part A 51*, L7–L21.
31. Powell, R. M. (2001) Ph.D. Thesis, University of Nebraska, Lincoln, NE.
32. Marquardt, D. (1963) An algorithm for Least-Squares Estimation of Nonlinear Parameters. *SIAM J. Appl. Math. 11*, 431–441.
33. Durbin, J., and Watson, G. S. (1950) Testing for serial correlation in least squares regression, I. *Biometrika 37*, 409–428.
34. Swed, F. S., and Eisenhardt, C. (1943) Tables for testing randomness of grouping in a sequence of alternatives. *Ann. Math. Stat. 4*, 66–87.
35. Parkhurst, L. J. (2004) Distance parameters derived from time-resolved Forster resonance energy transfer measurements and their use in structural interpretations of thermodynamic quantities associated with protein-DNA interactions. *Methods Enzymol. 379*, 235–262.
36. Parkhurst, L. J., Parkhurst, K. M., Powell, R., Wu, J., and Williams, S. (2001) Time-resolved fluorescence resonance energy transfer studies of DNA bending in double-stranded oligonucleotides and in DNA-protein complexes. *Biopolymers 61*, 180–200.
37. Akaike, H. (1970) Statistical Predictor Identification. *Ann. Inst. Stat. Math. 22*, 203–217.
38. Akaike, H. (1973) A new Look at Statistical Model Identification. *Trans. Automat. Contr. 19*, 716–723.
39. Garland, C. W., Nibler, J. W., and Shoemaker, D. P. (2003) *Experiments in Physical Chemistry*, 7th ed., pp 737−738, McGraw-Hill, Boston.
40. Bevington, P. R., and Robinson, D. K. (1992) *Data Reduction and Error Analysis for the Physical Science*, 2nd ed., pp 204−207, McGraw-Hill, New York.
41. Lee, T. I., and Young, R. A. (1998) Regulation of gene expression by TBP-associated proteins. *Genes Dev. 12*, 1398–1408.
42. Sethy-Coraci, I., Moir, R. D., Lopez-de-Leon, A., and Willis, I. M. (1998) A Differential Response of Wild Type and Mutant Promoters to TFIIB70 Overexpression in vivo and in vitro. *Nucleic Acids Res. 26*, 2344–2353.
43. Nikolov, D. B., Chen, H., Halay, E. D., Hoffman, A., Roeder, R. G., and Burley, S. K. (1996) Crystal structure of a human TATA box-

binding protein/TATA element complex. *Proc. Natl. Acad. Sci. U.S.A. 93*, 4862–4867.
44. DeDecker, B. S., O'Brien, R., Fleming, P. J., Geiger, J. H., Jackson, S. P., and Sigler, P. B. (1996) The crystal structure of a hyperthermophilic archaeal TATA-box binding protein. *J. Mol. Biol. 264*, 1072–1084.
45. Kao, C. C., Lieberman, P. M., Schmidt, M. C., Zhou, Q., Pei, R., and Berk, A. J. (1990) Cloning of a transcriptionally active human TATA binding factor. *Science 248*, 1646–1650.
46. Khrapunov, S., Pastor, N., and Brenowitz, M. (2002) Solution structural studies of the *Saccharomyces cerevisiae* TATA binding protein (TBP). *Biochemistry 41*, 9559–9571.
47. Whittington, J. E., and Parkhurst, L. J. (2008) Direct observation of Coordinated DNA bending and TATA binding Protein Conformational Changes. 2008 Biophysical Society Meeting Abstracts. *Biophys. J. 94* (Suppl.), 2018-Pos.
48. Wobbe, C. R., and Struhl, K. (1990) Yeast and human TATA-binding proteins have nearly identical DNA sequence requirements for transcription in vitro. *Mol. Cell. Biol. 10*, 3859–3867.
49. Press, W. H., Flannery, B. P., Teukolsky, S. A., and Vetterling, W. T. (1989) *Numerical recipes: The art of scientific computing*, pp 529−532, Cambridge University Press, New York.

BI8018724